Sensors and Actuators A 294 (2019) 17–24

Contents lists available at ScienceDirect

Sensors and Actuators A: Physical

journal homepage: www.elsevier.com/locate/sna

Role of oxygen vacancies in vanadium oxide and oxygen functional groups in graphene oxide for room temperature CO_2 gas sensors

Shrouk E. Zaki [a,1], Mohamed A. Basyooni [b,c,d,1], Mohamed Shaban [c,*], Mohamed Rabia [e], Yasin Ramazan Eker [f,*], Gamal F. Attia [d], Mucahit Yilmaz [a], Ashour M. Ahmed [c]

[a] Department of Theoretical Physics, Physics Research Division, National Research Centre, Dokki, Cairo, 12622, Egypt
[b] Department of Nano Science and Nano Engineering, Institute of Science and Technology, University of Konya Necmettin Erbakan, Konya 42060, Turkey
[c] Nanophotonic and Applications (NPA) Lab, Department of Physics, Faculty of Science, Beni-Suef University, Beni-Suef 62514, Egypt
[d] Space Research Laboratory, Solar and Space Research Department, National Research Institute of Astronomy and Geophysics (NRIAG), Helwan, Cairo, Egypt
[e] Polymer Research Laboratory, Chemistry Department, Faculty of Science, Beni-Suef University, Beni-Suef 62514, Egypt
[f] Department of Metallurgy and Material Engineering, Faculty of Engineering and Architectural, Necmettin Erbakan University, Konya, Turkey

ARTICLE INFO

Article history:
Received 27 March 2019
Received in revised form 16 April 2019
Accepted 25 April 2019
Available online 27 April 2019

Keywords:
Graphene oxide
Vanadium oxide
Gas sensor
Hummers method
Oxygen vacancies
Response and recovery time

ABSTRACT

The greenhouse effect is involving global heating and climate change within the world. Carbon dioxide (CO_2) is one of the major gas at the origin of this effect, but also the byproduct of human activity. Therefore, monitoring the indoor/outdoor CO_2 emission by gas sensors is one of the priorities for environmental preservation. In this paper, the sensing performance of CO_2 towards two different O-rich films have been studied; graphene oxide (GO) and vanadium dioxide (VO_2). The preparation of GO film has been carried out by spray pyrolysis on fluorine tin oxide (FTO) prepared by the modified Hummers method. While the VO2 film has been sol-gel spin-coated on a glass substrate. Both films have been characterized using XRD, SEM and electrical properties. The CO_2 gas sensing mechanism and the role of oxygen vacancies in VO_2 are addressing. The oxygen functional groups in GO play a main role in the CO_2 gas the sensitivity level and response time. Their gas sensing performances have been investigated based on measuring the response vs recovery time, dynamic response curve analysis and sensitivity. In order to better understand the sensing mechanism, characterization has been done with different gas concentrations. Both GO and VO_2 based CO_2-sensors are acted as an n-type sensor. Sensing behavior of GO at RT has explained to be mainly mediated by the oxygen functional groups and a wide range of active sites. In the other hand, VO_2 contains oxygen vacancies and more defect sites which play a main role in the RT sensing activity and low recovery time.

© 2019 Elsevier B.V. All rights reserved.

1. Introduction

CO_2 is considered one of the primary greenhouse gases emitted in the daily activities, which effect on the global warming and climate change. Monitoring and detection of CO_2 have attracted researches with especial concern on the room temperature (RT) and low-power gas sensors for different applications such as; air-quality monitoring, air-conditioners, agricultural production, clean energy technologies, engine exhausts, chemical industry [1,2]. Recently, TiO_2 nanoparticles on fabric surfaces can remove volatile compounds by converting them to carbon dioxide [3–5] for in-door and out-door CO_2 detection application. The widely used infrared gas detection technology are getting limited because of the IR instruments are usually large and expensive [6]. Concerning CO_2, their chemical stability makes it more difficultly detectable comparing to the other reductive gases especially for room temperature detection. chemiresistor sensor is based on a change in the electrical resistance of metal oxides within their structure upon gas exposure [7].

Three kind of materials have been usually studied in the literature for CO_2 gas sensing; metal-oxides (ZnO, TiO_2, SnO_2 or CeO_2), noble metal like Pd or Au, and graphene-based materials (quantum dots, double layer graphene or doped graphene nanosheet). The common ZnO film have been prepared by chemical spray pyrolysis given a high response of 64% sensitivity with a response and recovery time of 75 and 108 s, respectively for 400 ppm CO_2 gas

* Corresponding authors.
E-mail addresses: mssfadel@aucegypt.edu (M. Shaban), yeker@erbakan.edu.tr (Y.R. Eker).
[1] These authors are equally contributors.

https://doi.org/10.1016/j.sna.2019.04.037
0924-4247/© 2019 Elsevier B.V. All rights reserved.

concentration at 350° C [8]. In our recent work in ZnO, the gas detection has been successfully carried out at RT with 81.9% sensitivity with a response and recovery times of 283 and 472 s respectively at 50 sccm CO_2, thanks to Na-doped ZnO thin films [9]. Even if the working temperature has been down to the room temperature with the Na-doped sensor, the dynamic parameters have been prolonged i.e. the response and recovery time are too long. CeO_2 and Gd-doped CeO_2 powder has been also tested at 250° C with a sensitivity of 45% by using the doped oxide [10]. Concerning Pd and Au-decorated-Silicon nanowires-based sensors, very interesting results have been obtained with a 111 s response time and 82 s recovery times. However minimum gas pressure is needed and also the sensor preparation is complex and used expensive materials [10]. In the case of graphene-based material, results obtained with 10 nm quantum dots are not clearly observable, whatever the preparation of material is too complex [11]. Double-layer graphene with a fast response and recovery times showed a limited sensitivity [12]. Finally, Fe-doped graphene has been theoretically investigated as well [13].

Based on our literature survey, the application of GO and VO_2 for CO_2 sensors have not been studied. However, both have been used for other gas sensing applications and gave remarkable results. For examples, Prasa et al., investigated the CH_4 sensitivity in the semiconductor state of VO_2 (at 50° C) and in the metallic phase (at 150 °C) with sensitivity of 1.4% and 0.7% at 100 ppm, respectively [14]. He et al. thermodynamically demonstrated high stability of VO_2 at RT towards C_2H_2 [15]. Also palladium decorated VO_2 for H_2 detection has studied [16].

GO is the intermediate product during the synthesis of graphene-based materials via Hummer's method. It is obtained after the strong oxidation of graphite containing, therefore too many oxygen functional groups at the surface as used in our previous study [17]. These functional groups play a key role in the gas adsorption kinetics, involving the change of their electrical or optical properties with exposure to certain gases [18] such as humidity [19], alcohols [20] and ammonia [21]. VO_2 is an archetypal correlated oxide material, exhibits semiconductor-metal transition (SMT) at about 68° C [22]. At ambient pressure, below the transition temperature (T_c), VO_2 has a monoclinic (M1 phase), with space group $C12/m1$ (12) [23] and lattice constants a ≈ 9.08 Å, b ≈ 5.76 Å, c ≈ 4.53 Å, $\beta = 90.3^{o}$ [24]. Above the T_c, VO_2 adopts a tetragonal rutile (R) structure with space group of $P4_2\,mnm$ (136) and a lattice constants $a = b \approx 4.55$Å, $c \approx 2.85$Å [24,25]. Different synthesis approaches have addressed to control the oxidation of vanadium and oxygen in the V—O compounds such as pulsed dc magnetron sputtering [14], thermolysis [26], hydrothermal [27], sol-gel [28], and PLD [29]. Among them, sol-gel process is a facile and cheap method for VO_2 preparation where a V^{5+} or V^{4+} precursor is firstly prepared, and then the precursor is transferred onto a hydrophilic substrate through dip/spin coating. Finally, the VO_2 phase is formed by a high temperature annealing process under inert atmosphere, e.g. vacuum or N_2/Ar/CO_2.

In this report, both GO prepared via modified Hummer's method and the monoclinic semiconductor phase of VO_2 have been tested towards CO_2 gas sensitivity at RT. By correlating the physical and chemical characterization and the sensing measurements, clues to explain the sensing performance have been investigated.

2. Experimental part

2.1. Materials

Graphite fine powder was purchased from Alpha Chemika, Mumbai. $KMnO_4$ and H_2SO_4 were purchased from El Nasr chemical company, Egypt. H_2O_2 and H_3PO_4 were purchased from Pio Chem Company, Egypt. Dimethyl sulfoxide (DMSO) and V_2O_5 powder (99.5%) were purchased from Sigma–Aldrich.

2.2. Synthesis of graphene oxide

The preparation of GO was carried out by the modified Hummers method [30],details are described in our previous work [31]. Shortly, 1.0 g of graphite powder was added over mixture of 120 and 14 ml of concentrated H_2SO_4 and H_3PO_4, respectively. The process took place in an ice bath, and then 6 g of $KMnO_4$ was added over them slowly for 1 h under the effect of the magnetic stirrer. The solution mixture was leaved for 24 h over the magnetic stirrer at 50° C. Then 800 ml of H_2O_2 (0.05 M) was added over them drop by drop in an ice bath to reduce the residual of the $KMnO_4$. The mixture released a large amount of bubbles and the color of the mixture changed into brilliant yellow. For further purification, the as-obtained graphene oxide was re-dispersed in DI water and then was dialyzed for one week to remove any residual salts and acids.

2.3. Synthesis of vanadium dioxide

0.3 g V_2O_5 powder was dissolved in 30 mL hydrogen peroxide (30%) at RT under continuous stirring until a homogeneous reddish-brown color formed. After short time, a dark red sol was formed due to the harsh boiling caused by a self-heating. Then, the solution aged at RT for couple of days until a homogeneous dark red gel was formed [32].

2.4. Preparation of GO and VO_2 films

The GO film was prepared on FTO while VO_2 film was prepared on SiO_2/Si substrate with a dimension of 1 x 2 cm. Both substrates were cleaned in Acetone and IPA separately for 30 min in ultrasonic water path at RT, then washed by DI water and dried well in N_2 environment before the deposition. The GO solution (11 mg/ml) was sprayed at 200° C by the spray pyrolysis system with the rate of 50 μm L/min for 20 min over FTO glass. Concerning VO_2 film, a small portion of the solution was spin coated on the SiO_2/Si substrate, at a suitable speed of 2500 rpm for 1 min, then transferred into a quartz tube furnace on a quartz crucible. After evacuating the tube at $1*10^{-2}$ Torr, 200 sccm N_2 gas was settled for 3 h at 450° C.

2.5. Characterization of the prepared samples

The crystal structure of the deposited GO and VO_2 were studied using high-resolution X-ray diffractometer system (model: PANalytical X'Pert Pro, Holland) with CuK α radiation (λ = 1.5406 A°), operated at 45 kV and 40 mA. The XRD patterns of GO and VO_2 were recorded in the 2θ range 10-80° and 10-60°, respectively. The pattern was analyzed by matching the observed peaks with the standard patterns provided by JCPDS files. Later, structure parameters were determined via Rietveld structure refinement of VO_2 film using FULLPROF program [33]. Morphological analysis was carried out using SEM (Model: ZEISS SUPRA 55 V P and ZEISS LEO, Gemini Column). The UV–vis measurements were done by using Shimadzu UV spectrophotometer (M160 PC) at RT in the range 200–900 nm for GO dispersed within DMSO. The FTIR measurement of GO was carried out using Shimadzu FTIR-340 Jasco spectrophotometer.

2.6. Gas sensing system

The details of the testing system and gas sensing parameters were reported in our previous work [9], which can be summarized as follow: a home-made airtight glassy gas chamber with two gas sources (CO_2 and N_2) input, exhaust gas output and two electrical wires input where the testing films are connected. A conducting

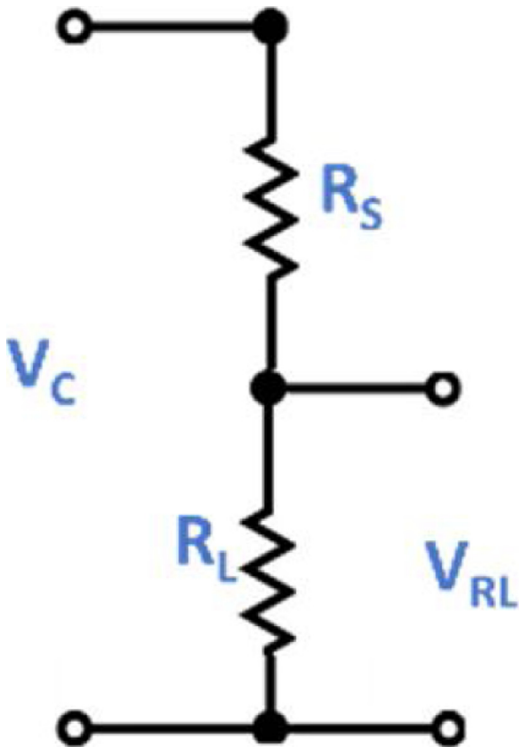

Fig. 1. Gas sensor electrical circuit.

silver paste was used to make ohmic contacts on both ends and collect the output sensor signals. Since the measurements were done at RT, just a load resistor (R_L) was connected in series with the sensor as shown in Fig. 1. An input voltage (V_C) of 1 V was applied from DC power supply (IMPO 11.11, 30 V/3 A). The output voltage (V_{out}) was taken across R_L and recorded using Fluke Digital Multimeters 287/289 interfaced with a computer, whereas gases were switched on/off at each cycle. N_2 was used through the sensor chamber to stabilize the sensor resistance during each cycle.

By collecting the output voltage, the sensor resistance R_S can be calculated using Eq. (1) [9];

$$R_S = \frac{V_c - V_{out}}{V_{out}} R_L \quad (1)$$

The sensor response (sensitivity %) was calculated using Eq. (2) [9]:

$$S(\%) = \left| \frac{R_{CO_2} - R_{N_2}}{R_{N_2}} \right| \times 100 \quad (2)$$

Where R_{CO_2}, R_{N_2} are the sensor resistances in the presence of CO_2 and N_2, respectively.

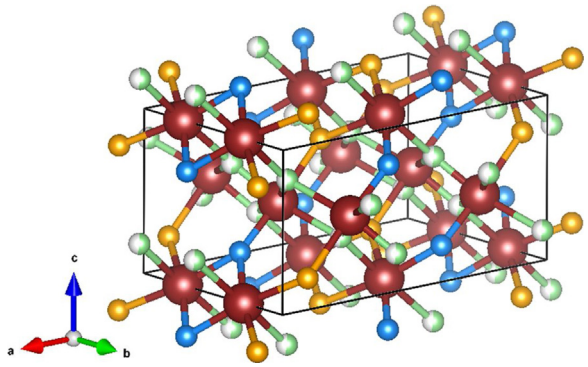

Fig. 3. Monoclinic structure of VO_2. Large red spheres denote V atoms and small orange, green and blue spheres denote O atoms at O1, O2, and O3 positions, respectively (For interpretation of the references to colour in this figure legend, the reader is referred to the web version of this article.).

3. Results and discussions

3.1. Films structure

The spin coated V_2O_5 based solution has been pyrolyzed under N_2 atmosphere at 450° C for 3 h. The XRD analysis of this film shown a (110) main peak at $2\theta \approx 28°$, Fig. 2(b). This peak is characteristic of VO_2(B) which is the one of the monoclinic allotropes of VO_2 based material confirming that the heat treatment successfully transformed the starting structure. Moreover, the sharpness and the intensity of this peak demonstrates a high film crystallinity. Four other important peaks at 37°, 42°, 55° and 57° related to (211), (210), (220) and (022) respectively. These indices were determined by JCPDS Card No. 72-0514. At the same time, lattice degrees of freedom are important for the different phases of VO_2. Therefore, structural analysis of VO_2 was performed with FULLPROF program. Experimental and calculated pattern, background, difference between calculated and experimental pattern and Bragg positions show in Fig. 2(b). After the determination of the initial parameters for the Rietveld refinement [34,35], lattice parameters and atom coordinates were determined. The monoclinic structure of semiconducting phase of VO_2 is based on a monoclinic lattice and it has C12/m1 symmetry with space group VO_2. As a result of the calculation, the unit cell parameters were found as a = 9.10739, b = 5.75095, c = 4.49124 Å and angles between the axes $\alpha = 90°$, $\beta = 90.3431°$, $\gamma = 90°$. However, the Wyckoff position of metal atoms are (2a): (0,0,0) and (4f): (0.25, 0.25, 0.25) and oxygen atoms are (4i): (0.175, 0, 0.25), (0.175, 0.5, 0.25) and (8j): (0.075, 0.25, 0.75). The monoclinic phase of VO_2 is shown in Fig. 3. The unit cell parameters and atomic coordinates were pretty close to the reference values which were selected [23] due to the amount of oxygen vacancies in the structure. As a result of the calculations, the occupations of vanadium and oxygen in the structure were found to be 2.034 and

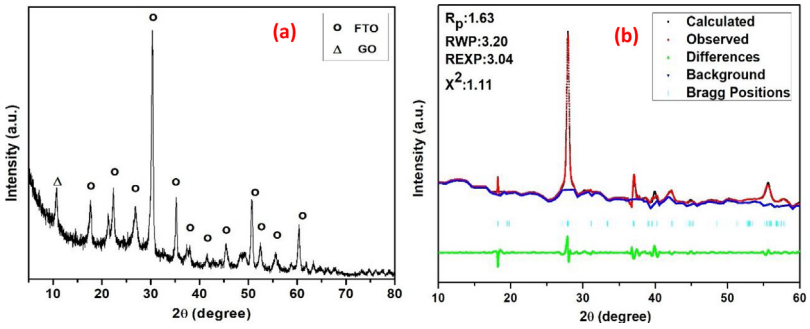

Fig. 2. XRD spectra of GO (a) and VO_2 (b) film.

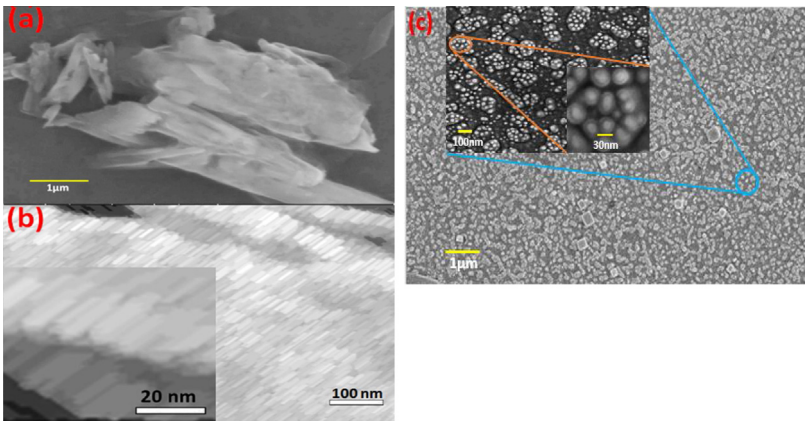

Fig. 4. SEM images of GO **(a–b)** and VO_2 **(c)** films.

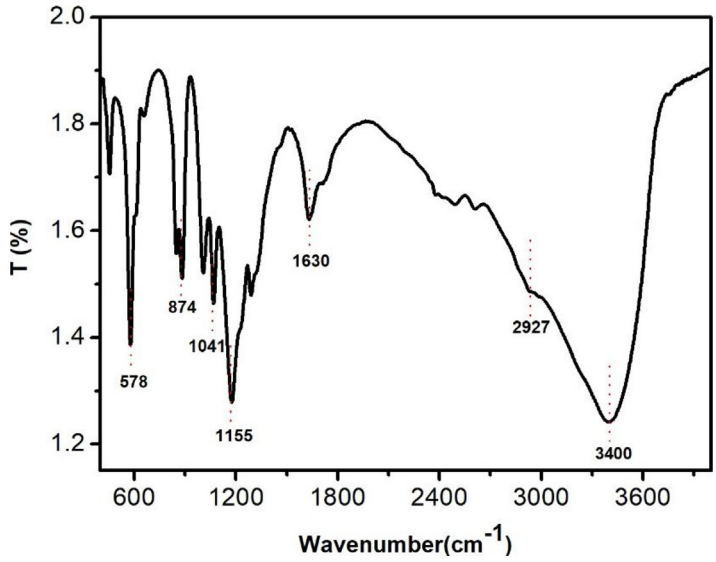

Fig. 5. FTIR spectrum of GO film at RT.

3.519, respectively. The calculated amount of oxygen: vanadium (O:V) in the VO_2 compound indicating that more oxygen vacancies and defects are presented. Oxygen deficient vanadium oxide ($VO_{2-\delta}$) have reported many times to stabilize the metal state [36], to decrease the SMT [37] and to narrow the band gap in the monoclinic phase [38]. Oxygen vacancies are electron donors with n-type conductivity which can change the electron orbital occupancy and band structures and contribute to the high gas respectively at RT [39]. The particle size of VO_2 has been calculated to be $\tilde{2}3$ nm using Debye-Scherrer equation $D = \frac{0.9\lambda}{W.cos\theta}$; where W is the full width at half maximum (FWHM) which was calculated around the main peak (27.93°) using Lorentz fitting and equal to 0.354, θ is the Bragg's angle, λ is the X-ray wavelength (CuKα = 0.15405 nm).

Concerning the GO deposited at relatively low temperature of 200 °C by spray pyrolysis, the characteristic peak of carbon at 10,8° is observed and it corresponds to definite d-spacing of 0.823 nm [31] as shown in Fig. 2(a). The mean dimension of an ordered stack of graphene oxide sheets in GO film that are oriented perpendicularly to the diffracting plane is calculated from the FWHM of the XRD peak using the Debye–Scherrer equation as mentioned above with a particle size of 41 nm.

3.2. Films morphology

Fig. 4 (a–b) shows the SEM morphology of GO sheets at different scales which reveals a wrinkle 2D structure. The porous 2D structure shows a high possibility for gas adsorption which can play a main role in the sensing behavior at room temperature as shown in Fig. 4 (a). Fig. 4(b) shows a high resolution of the ordered stacks of GO sheets. While for VO_2 film, a well distributed clusters with a particle size around 27 nm is observed as shown in Fig. 4(c). The high amount of VO_2 particles denotes highly divided surface area which is an advantage for gas adsorption enhancements.

3.3. Structural properties of GO film

3.3.1. Functional groups

The GO was prepared via oxidation of graphite based on modified of Hummer's method, thereafter the film was formed by spray pyrolysis at 200 °C. Both steps are favoring the oxidation of carbon materials which is required for the gas sensing performance. The FTIR spectrum of the GO film reveals the presence of oxygen functions, Fig. 5.

The wide peak at about 3400 cm^{-1} is assigned to the bonded O—H stretching vibration, the one at 1630 cm^{-1} is assigned to C=O carbonyl group while those at 1155 and 1041 cm^{-1} are related to the C—O epoxide groups [40–42]. All these peaks demonstrate that GO film contains an important amount of oxygen atoms under different functional groups which will investigated towards CO_2 interaction and sensing.

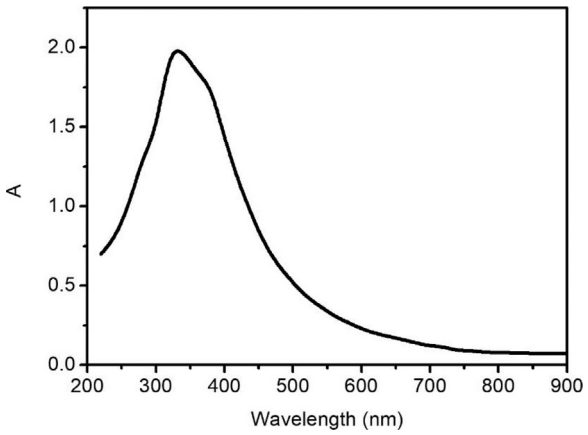

Fig. 6. Shows the optical absorption of the GO film.

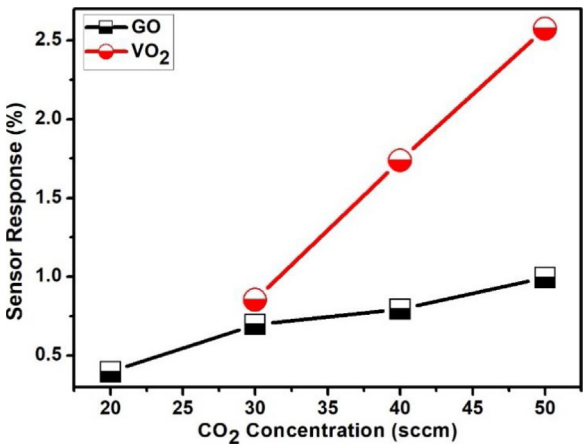

Fig. 8. Sensitivity of VO_2 and GO films at RT towards different CO_2 concentrations.

3.3.2. Aromatic group

The UV absorption spectrum shows a strong and wide absorption band centered around 335 nm as shown in Fig. 6 which is originated from different inter- and intra-band. Therefore, this peak is attributed to π-π* transition of the aromatic C—C ring and n-π* transition of C═O bond [31,43]. The GO film is therefore containing an important amount of aromatic structures which plays a crucial role to the conductivity of carbon-based materials.

3.4. I-V and sensors sensitivity

The presence and the concentration of gases are proportionally affecting the resistance/conductivity change of films [44]. The current-voltage (I-V) measurements of GO and VO_2 films at RT clearly show linear Ohmic behavior as shown in Fig. 7(a). According to the Ohm law, the conductivity and resistivity values for films can be calculated by using the curve slopes and their reverse value respectively. In presence of 100 sccm CO_2 the resistivity of GO film (15 MΩ) is ten times lower than the one of VO_2 film (153 MΩ). Similarly, with 100 sccm N_2, the resistivity of GO film (29 MΩ) is almost ten times lower than the one of VO_2 film (275 MΩ). These differences clearly demonstrate the effect of gas adsorption on the film resistivity and their ability to detect CO_2 gas presence. The resistance difference according to the gases with GO film is 14 MΩ, while it is 122 MΩ with VO_2 film. These values show that the VO_2 based sensor is more sensitive towards CO_2 concentration than the GO based sensor in presence of 100 sccm gas, the same behavior is depicted on Fig. 8 for high concentration.

By using these electrical responses with different gas concentration and by applying Eqs. (1) and (2), differences in gas sensitivity was obtained as illustrated in Fig. 8. For both materials the sensitivity is increasing with the gas concentration. However, the VO_2 film sensitivity is better at high gas concentration, while GO film sensitivity is working well at low gas concentration.

3.5. Sensor dynamics

The sensor response time toward the presence of CO_2 is an important parameter to estimate the material performance. In fact, it determines not only the delay to reach the exact value of gas concentration but also the time requested to prepare the sensor for the next measurement. The sensor response has been evaluated with different CO_2 concentrations from 20 to 50 sccm as illustrated in Fig. 9(a) and (b). In each case, the resistance of the sensor is increasing with the CO_2 concentration up to reach a highest value which also increases according to the CO_2 concentration. On contrarily, the sensor resistance is decreasing down to lowest baseline value via the introduction of the stabilizing N_2 gas. The response time (t_{res}) is defined as the time taken for the relative resistance change to reach 90% of the steady state value after the CO_2 is injected (*green continuous line*). Whereas the recovery time is for the delay required to reduce by 90% the difference between highest and lowest resistance (*turquoise dotted line*).

Both response and recovery time for GO and VO_2 based sensor are prolonged with the increase of CO_2 concentration (Fig. 10). For GO based sensor, the recovery time is always longer than the response time. However, the response time is quasi-linearly increasing with CO_2 concentration, whereas for the recovery time two different evolution is observed. Especially, at 20 sccm the recovery time is ~50% shorter than with 30 sccm CO_2. This behavior suggests that the CO_2 sensing is related to at least two interaction phenomena. For VO_2 based sensor, the response time is always longer than the recovery time. Similarly, to GO based sensor, the response time follow a quasi-linear evolution with the CO_2 concen-

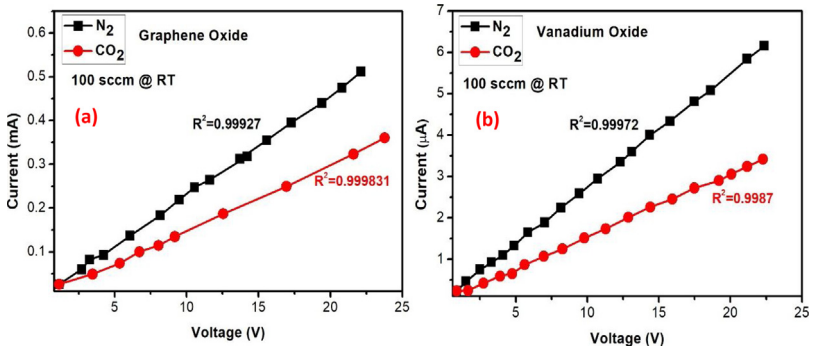

Fig. 7. I-V curve of GO (a) and VO_2 (b) films.

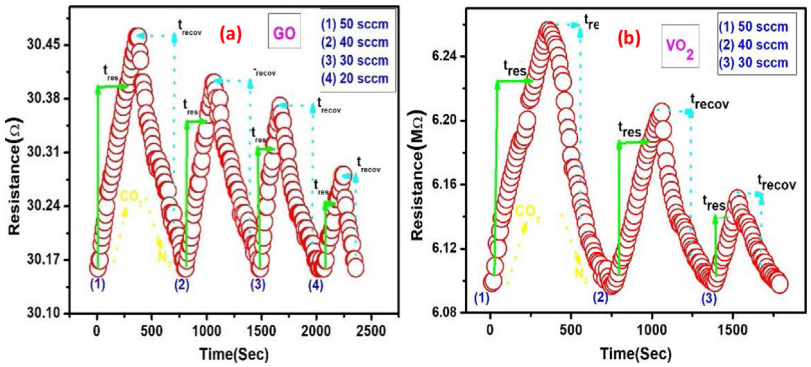

Fig. 9. Dynamic response of GO (a) and VO_2 (b) films for different CO_2 concentrations at RT.

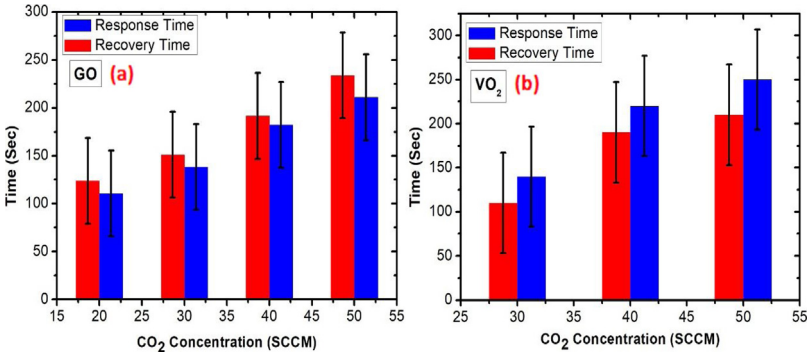

Fig. 10. The response and recovery times of GO (a) and VO_2 (b) films for CO_2 gas.

tration, but for the recovery time there is still a breakpoint inducing also two different interaction phenomena.

The detection limit (DL) can be calculated from the linear calibration curve by calculating standard deviation (SD) of the sensor sensitivity [9,45], DL = 3*SD/slope. The calculated DL for GO and VO_2 are 0.34096 and 0.52328 sccm, respectively. The limit of quantification (LOQ) is defined as the lowest acceptable concentration of CO_2 on GO and VO_2 that can be detected with high accuracy and precision [45]. By considering the standard signal-to-noise ratio (10:1), the LOQ can be defined as LOQ = 10*SD/slope. The calculated LOQ for GO and VO_2 are 1.17311 and 1.66186 sccm, respectively.

3.6. *Sensing mechanism of GO and VO_2 based CO_2 gas sensors at RT*

Four different adsorption mechanisms are presented in the literature [46–49]. (i) the capillarity which requires relevant pores at the adsorbent surface, (ii) the electrostatic effect involving the presence of metal oxide adsorbent, (iii) the π-π interaction between double bonds present both in adsorbent and in adsorbate and (iv) the weak hydrogen bonds between hydrogen and electronegative atom possessing valence electron doublets. In this purpose, the study of adsorbate and the adsorbent properties are required to clarify the adsorption mechanisms for both materials.

The adsorbate CO_2 is a linear polar molecule consists of 2 symmetric dipoles where negative and positive pole centers are overlay. Both oxygens are connected to the carbon atom with two double π-bond ($O^{\ominus}=C^{\oplus}=O^{\ominus}$). Known as an oxidizing agent, in other words CO_2 is able to take electrons from the metal oxide film surfaces increasing the number of holes and therefore the film resistance [9].

Vanadium oxide is considered as a semiconductor-metal phase transition material due to the involving electron-electron correlated interaction. Near RT, VO_2 behaves as a semiconductor oxide with relatively lower resistance when compared to other metal oxides. The XRD refinement analysis showed that the VO_2 film contains oxygen vacancies and defects. These oxygen vacancies act as an electron donor centers, so VO_2 becomes as a n-type semiconductor which clear from the I-V curve and adsorption-desorption kinetic curves in Figs. 7 and 9(b). Moreover, the nanoparticle clusters of VO_2 involve a high surface energy and high reactivity which mainly contribute to the RT sensing behaviour as predicted in ZnO [9]. The O-rich adsorbate (CO_2) is chemisorbed during its interaction with O-depleted adsorbent surface. The chemisorbed oxygen will catch electrons from the conduction band by forming O^{2-} and increase the depletion region and consequently the overall resistance as predicted by Barsan et al [47]. The evolution of the response time (adsorption) is almost linearly proportional to the gas concentration. During the desorption, the introduction of N_2 involves the releasing of the trapped electrons to the conduction band and increased the film conductivity. The concentration of oxygen vacancies in VO_2 plays a main role in the adsorption-desorption kinetics as indicated in Fig. 10 (b). However, the desorption is faster than adsorption, this effect is probably due to strong attraction of the adsorbate by the numerous defect which delayed the desorption under N_2 atmosphere. On the other hand, in this situation, the chemisorption (with CO_2) as well as the desorption (with N_2) are longer but the difference is low. The diffusion of both gases can be considered as quite similar during the whole process.

Concerning GO, the response time is shorter than the recovery time which is characteristic to a strong attraction of the CO_2. It confirms the results previously reported indicating the difficulty to desorb CO_2 easily adsorbed on GO/ITO film [42]. Moreover, comparing to VO_2 the higher sensitivity of the GO film is reinforced by firstly the ability to detect the presence of CO_2 up to 20 sccm in atmosphere. Secondly, both materials present approximately the same response delay with 30 sccm CO_2 in atmosphere, while the response time of 50 sccm with GO is comparable to the one of VO_2

with 40 sccm CO_2. These observations show that (i) the active sites for both materials have not the same accessibility, (ii) the most affordable sites are not fully used at 30 sccm CO_2 and (iii) CO_2 must diffuse along or within VO_2 to reach not readily available sites.

Regarding the sensing mechanism, the presence of hydrogenated oxygen functions at the GO surface as well the π bonds within its structure seems to be the main reasons. In fact, CO_2 includes two oxygen atoms with electron pair convenient for the hydrogen bonds. Moreover, oxygens are double bonded to the central carbon which can favour the π-π interactions [15] also describe for the sensing of CO_2 on the graphene surface [42]. These results are reinforced by the literature, where remarkable performance of GO sensing towards H_2 [50] and NO_2 [51,52] have been reported. H_2 is favouring the formation of hydrogen bonds with oxygens present at the surface of GO, while NO_2 gas structure includes one single and one double bond.

4. Conclusions

A simple and effective synthesis strategy to prepare GO and VO_2 have been demonstrated in this study. For both materials, the oxygen concentration plays a crucial role either by its presence as hydrogenated functions on the GO surface or its deficiency within the VO_2 structure. Both situations involve the adsorption of CO_2 which is allow the detection of CO_2. However, GO based sensor can virtually sense up to 20 sccm CO_2 present in N_2, while VO_2 based can only detect 30 sccm gas present in N_2. This sensitivity difference is explained by the adsorption-desorption mechanisms variation which are related not only to the material properties, but also to their morphology. This study may open a new venue to fabricate VO_2 and GO nanostructures for potential applications in environmental monitoring and gas detection.

Acknowledgments

The authors declare no financial support is providing for this work.

References

[1] K.-Q. Peng, X. Wang, S.-T. Lee, Gas sensing properties of single crystalline porous silicon nanowires, Appl. Phys. Lett. 95 (2009) 243112, http://dx.doi.org/10.1063/1.3275794.
[2] S. Naama, T. Hadjersi, A. Keffous, G. Nezzal, CO<inf>2</inf> gas sensor based on silicon nanowires modified with metal nanoparticles, Mater. Sci. Semicond. Process. 38 (2015) 367–372, http://dx.doi.org/10.1016/j.mssp.2015.01.027.
[3] H. Memon, N. Kumari, Study of multifunctional nanocoated cold plasma treated polyester cotton blended curtains, Surf. Rev. Lett. 23 (2016), 1650036, http://dx.doi.org/10.1142/S0218625x16500360.
[4] H. Memon, S. Yasin, N.A. Khoso, S. Memon, Study of wrinkle resistant, breathable, anti-uv nanocoated woven polyester fabric, Surf. Rev. Lett. 23 (2015), 1650003, http://dx.doi.org/10.1142/S0218625x16500037.
[5] H. Memon, N. Kumari, A.W. Jatoi, N.A. Khoso, Study of the indoor decontamination using nanocoated woven polyester fabric, Int. Nano Lett. 7 (2016) 1–7, http://dx.doi.org/10.1007/s40089-016-0194-7.
[6] L. Joly, B. Parvitte, V. Zeninari, G. Durry, Development of a compact CO2 sensor open to the atmosphere and based on near-infrared laser technology at 2.68 μm, Appl. Phys. B 86 (2007) 743–748, http://dx.doi.org/10.1007/s00340-006-2568-4.
[7] D. Wang, Y. Chen, Z. Liu, L. Li, C. Shi, H. Qin, J. Hu, CO2-sensing properties and mechanism of nano-SnO2 thick-film sensor, Sens. Actuators B Chem. 227 (2016) 73–84, http://dx.doi.org/10.1016/J.SNB.2015.12.025.
[8] Y.M. Hunge, A.A. Yadav, S.B. Kulkarni, V.L. Mathe, A multifunctional ZnO thin film based devices for photoelectrocatalytic degradation of terephthalic acid and CO2 gas sensing applications, Sens. Actuators B Chem. 274 (2018) 1–9, http://dx.doi.org/10.1016/J.SNB.2018.07.117.
[9] M.A. Basyooni, M. Shaban, A.M. El Sayed, Enhanced gas sensing properties of spin-coated Na-doped ZnO nanostructured films, Sci. Rep. 7 (2017) 41716, http://dx.doi.org/10.1038/srep41716.
[10] A.A. Aboud, H. Al-Kelesh, W.M.A. El Rouby, A.A. Farghali, A. Hamdedein, M.H. Khedr, CO2 responses based on pure and doped CeO2 nano-pellets, J. Mater. Res. Technol. 7 (2018) 14–20, http://dx.doi.org/10.1016/J.JMRT.2017.03.003.
[11] D. Raeyani, S. Shojaei, S.A. Kandjani, W. Wlodarski, Synthesizing graphene quantum dots for gas sensing applications, Procedia Eng. 168 (2016) 1312–1316, http://dx.doi.org/10.1016/J.PROENG.2016.11.356.
[12] X. Fan, K. Elgammal, A.D. Smith, M. Östling, A. Delin, M.C. Lemme, F. Niklaus, Humidity and CO2 gas sensing properties of double-layer graphene, Carbon N.Y. 127 (2018) 576–587, http://dx.doi.org/10.1016/j.carbon.2017.11.038.
[13] D. Cortés-Arriagada, N. Villegas-Escobar, D.E. Ortega, Fe-doped graphene nanosheet as an adsorption platform of harmful gas molecules (CO, CO2, SO2 and H2S), and the co-adsorption in O2 environments, Appl. Surf. Sci. 427 (2018) 227–236, http://dx.doi.org/10.1016/J.APSUSC.2017.08.216.
[14] A.K. Prasad, S. Amirthapandian, S. Dhara, S. Dash, N. Murali, A.K. Tyagi, Novel single phase vanadium dioxide nanostructured films for methane sensing near room temperature, Sens. Actuators, B Chem. 191 (2014) 252–256, http://dx.doi.org/10.1016/j.snb.2013.09.102.
[15] Y.P. Ma, W. Xue, Z.C. Wang, M.F. Ge, S.G. He, Acetylene cyclotrimerization catalyzed by TiO2 and VO2 in the gas phase: a DFT study, J. Phys. Chem. A 112 (2008) 3731–3741, http://dx.doi.org/10.1021/jp711027z.
[16] J.M. Baik, M.H. Kim, C. Larson, C.T. Yavuz, G.D. Stucky, A.M. Wodtke, M. Moskovits, Pd-sensitized single vanadium oxide nanowires: highly responsive hydrogen sensing based on the metal−insulator transition, Nano Lett. 9 (2009) 3980–3984, http://dx.doi.org/10.1021/nl902020t.
[17] W.N. Nyairo, Y.R. Eker, C. Kowenje, E. Zor, H. Bingol, A. Tor, D.M. Ongeri, Efficient removal of lead(II) ions from aqueous solutions using methyl-β-cyclodextrin modified graphene oxide, Water Air Soil Pollut. 228 (2017) 406, http://dx.doi.org/10.1007/s11270-017-3589-9.
[18] K. Toda, R. Furue, S. Hayami, Recent progress in applications of graphene oxide for gas sensing: a review, Anal. Chim. Acta 878 (2015) 43–53.
[19] V.S. Palaparthy, H. Kalita, S.G. Surya, M. Shojaei, Graphene oxide based soil moisture microsensor for in situ agriculture applications, Sens. Actuators B Chem. 273 (2018) 1660–1669.
[20] S. Aslam, T. Hussain, T. Anwar, U. Khan, A. Nairan, K. Khan, Graphene oxide coated graphene foam based chemical sensor, Mater. Lett. 235 (2019) 66–70.
[21] T.N. Ly, S. Park, Highly sensitive gas sensor using hierarchically self-assembled thin fi lms of graphene oxide and gold nanoparticles, J. Ind. Eng. Chem. 67 (2018) 417–428.
[22] K. Karsli, Vanadium Oxide (Vo X) Thin Films Elaborated By Sol-Gel Method For Microbolometer Applications, A Thesis Submitted To The Graduate School Of Natural And Applied Sciences Of Middle East Technical University, 2012 (Accessed 19 December, 2018) Https://Etd.Lib.Metu.Edu.Tr/Upload/12614078/Index.Pdf.
[23] J. Galy, G. Miehe, Ab initio structures of (M2) and (M3) VO2 high pressure phases, Solid State Sci. 1 (1999) 433–448, http://dx.doi.org/10.1016/S1293-2558(00)80096-5.
[24] J.D. Budai, A. Tselev, J.Z. Tischler, E. Strelcov, A. Kolmakov, W.J. Liu, A. Gupta, J. Narayan, In situ X-ray microdiffraction studies inside individual VO2 microcrystals, Acta Mater. 61 (2013) 2751–2762, http://dx.doi.org/10.1016/j.actamat.2012.09.074.
[25] D.B. McWhan, M. Marezio, J.P. Remeika, P.D. Dernier, X-ray diffraction study of metallic V O 2, Phys. Rev. B 10 (1974) 490–495, http://dx.doi.org/10.1103/PhysRevB.10.490.
[26] S. Guan, A. Rougier, O. Viraphong, D. Denux, N. Penin, M. Gaudon, Two-step synthesis of VO $_2$ (m) with tuned crystallinity, Inorg. Chem. 57 (2018) 8857–8865, http://dx.doi.org/10.1021/acs.inorgchem.8b00753.
[27] S. Han, Z. Zou, S. Huo, Hydrothermal synthesis of Mn-doped VO $_2$ (B) as cathode material for lithium-ion battery, IOP Conf. Ser. Mater. Sci. Eng. 382 (2018), 022059, http://dx.doi.org/10.1088/1757-899X/382/2/022059.
[28] Y.-R. Jo, S.-H. Myeong, B.-J. Kim, Role of annealing temperature on the sol–gel synthesis of VO $_2$ nanowires with *in situ* characterization of their metal–insulator transition, RSC Adv. 8 (2018) 5158–5165, http://dx.doi.org/10.1039/C7RA10865F.
[29] T.-H. Yang, R. Aggarwal, A. Gupta, H. Zhou, R.J. Narayan, J. Narayan, Semiconductor-metal transition characteristics of VO2 thin films grown on c- and r-sapphire substrates, J. Appl. Phys. 107 (2010), 053514, http://dx.doi.org/10.1063/1.3327241.
[30] N.I. Zaaba, K.L. Foo, U. Hashim, S.J. Tan, W.-W. Liu, C.H. Voon, Synthesis of graphene oxide using modified hummers method: solvent influence, Procedia Eng. 184 (2017) 469–477, http://dx.doi.org/10.1016/j.proeng.2017.04.118.
[31] M. Shaban, M. Rabia, A.M.A. El-Sayed, A. Ahmed, S. Sayed, Photocatalytic properties of PbS/graphene oxide/polyaniline electrode for hydrogen generation, Sci. Rep. 7 (2017) 14100, http://dx.doi.org/10.1038/s41598-017-14582-8.
[32] N. Wang, S. Magdassi, D. Mandler, Y. Long, Simple sol-gel process and one-step annealing of vanadium dioxide thin films: synthesis and thermochromic properties, Thin Solid Films 534 (2013) 594–598, http://dx.doi.org/10.1016/j.tsf.2013.01.074.
[33] J. Rodríguez-Carvajal, Recent advances in magnetic structure determination by neutron powder diffraction, Phys. B Phys. Condens. Matter. 192 (1993) 55–69, http://dx.doi.org/10.1016/0921-4526(93)90108-I.
[34] V. Eyert, The metal-insulator transitions of VO2: a band theoretical approach, Ann. Der Phys. 11 (2002) 650–702, http://dx.doi.org/10.1002/1521-3889(200210)11:9<650::AID-ANDP650>3.0.CO;2-K.
[35] S. Westman, I. Lindqvist, B. Sparrman, G.B. Nielsen, H. Nord, A. Jart, Note on a phase transition in VO2, Acta Chem. Scand. 15 (1961) 217, http://dx.doi.org/10.3891/acta.chem.scand.15-0217.
[36] J. Zhang, Z. Zhao, J. Li, H. Jin, F. Rehman, P. Chen, Y. Jiang, C. Chen, M. Cao, Y. Zhao, Evolution of structural and electrical properties of oxygen-deficient

VO2 under low temperature heating process, ACS Appl. Mater. Interfaces 9 (2017) 27135–27141, http://dx.doi.org/10.1021/acsami.7b05792.
[37] X. Wang, Z. Wang, G. Zhang, J. Jiang, Insight into electronic and structural reorganizations for defect-induced VO2 metal-insulator transition, J. Phys. Chem. Lett. 8 (2017) 3129–3132, http://dx.doi.org/10.1021/acs.jpclett.7b01300.
[38] L. Chen, Y. Cui, S. Shi, B. Liu, H. Luo, Y. Gao, First-principles study of the effect of oxygen vacancy and strain on the phase transition temperature of VO2, RSC Adv. 6 (2016) 86872–86879, http://dx.doi.org/10.1039/c6ra19121e.
[39] S. Fan, L. Fan, Q. Li, J. Liu, B. Ye, The identification of defect structures for oxygen pressure dependent VO2 crystal films, Appl. Surf. Sci. 321 (2014) 464–468, http://dx.doi.org/10.1016/j.apsusc.2014.10.057.
[40] S.Y. Toh, K.S. Loh, S.K. Kamarudin, W.R.W. Daud, Graphene production via electrochemical reduction of graphene oxide: synthesis and characterisation, Chem. Eng. J. 251 (2014) 422–434, http://dx.doi.org/10.1016/j.cej.2014.04.004.
[41] W.J. Kim, C. Basavaraja, P.X. Thinh, D.S. Huh, Structural characterization and DC conductivity of honeycomb-patterned poly(ε-caprolactone)/gold nanoparticle-reduced graphite oxide composite films, Mater. Lett. 90 (2013) 14–18, http://dx.doi.org/10.1016/j.matlet.2012.09.007.
[42] S. Drewniak, R. Muzyka, A. Stolarczyk, T. Pustelny, M. Kotyczka-Morańska, M. Setkiewicz, Studies of reduced graphene oxide and graphite oxide in the aspect of their possible application in gas sensors, Sensors (Switzerland) 16 (2016) 103, http://dx.doi.org/10.3390/s16010103.
[43] S.M. Roy, N.N. Rao, A. Herissan, C. Colbeau-Justin, Polyaniline film-based wireless photo reactor for hydrogen generation through exciton mediated proton reduction, Polymer (Guildf) 112 (2017) 351–358, http://dx.doi.org/10.1016/j.polymer.2017.02.013.
[44] G. Yasin, M. Arif, M. Shakeel, Y. Dun, Y. Zuo, W.Q. Khan, Y. Tang, A. Khan, M. Nadeem, Exploring the nickel–graphene nanocomposite coatings for superior corrosion resistance: manipulating the effect of deposition current density on its morphology, mechanical properties, and erosion-corrosion performance, Adv. Eng. Mater. 20 (2018), 1701166, http://dx.doi.org/10.1002/adem.201701166.
[45] M. Shaban, K. Abdelkarem, A.M. El Sayed, Structural, optical and gas sensing properties of Cu 2 O/CuO mixed phase: effect of the number of coated layers and (Cr + S) co-doping, Phase Transit. (2019) 1–13, http://dx.doi.org/10.1080/01411594.2019.1581886.
[46] M. Batzill, U. Diebold, Surface studies of gas sensing metal oxides, Phys. Chem. Chem. Phys. 9 (2007) 2307–2318, http://dx.doi.org/10.1039/b617710g.
[47] N. Barsan, U. Weimar, Conduction model of metal oxide gas sensors, J. Electroceramics 7 (2001) 143–167, http://dx.doi.org/10.1023/A:1014405811371.
[48] C. Kim, Y.S. Choi, S.M. Lee, J.T. Park, B. Kim, Y.H. Lee, The effect of gas adsorption on the field emission mechanism of carbon nanotubes, J. Am. Chem. Soc. 124 (2002) 9906–9911, http://dx.doi.org/10.1021/ja026538h.
[49] S. Santucci, S. Picozzi, F. Di Gregorio, L. Lozzi, C. Cantalini, L. Valentini, J.M. Kenny, B. Delley, NO2 and CO gas adsorption on carbon nanotubes: experiment and theory, J. Chem. Phys. 119 (2003) 10904–10910, http://dx.doi.org/10.1063/1.1619948.
[50] I. Lee, B. Singh, G.-H. Kim, J.-H. Park, J. Wang, S. Rathi, H.-I. Joh, C.-H. Lee, S. Maeng, Dielectrophoresis of graphene oxide nanostructures for hydrogen gas sensor at room temperature, Sens. Actuators B Chem. 194 (2014) 296–302, http://dx.doi.org/10.1016/j.snb.2013.12.009.
[51] H.J. Park, W.J. Kim, H.K. Lee, D.S. Lee, J.H. Shin, Y. Jun, Y.J. Yun, Highly flexible, mechanically stable, and sensitive NO2 gas sensors based on reduced graphene oxide nanofibrous mesh fabric for flexible electronics, Sens. Actuators, B Chem. 257 (2018) 846–852, http://dx.doi.org/10.1016/j.snb.2017.11.032.
[52] M.M. Ramli, S.S.M. Isa, M.F. Jamlos, S.A.Z. Murad, M.M. Isa, S.R. Kasjoo, N. Ahmad, N.I.M. Nor, N. Khalid, Few-layers graphene oxide for NO2 gas sensor on plastic, AIP Conf. Proc. (2017), http://dx.doi.org/10.1063/1.4975273, p. 020040.

Biographies

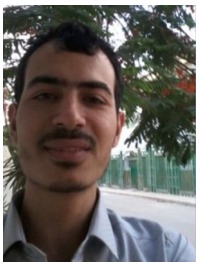

Shrouk E. Zaki is assistant researcher at physics research division in the National Research Center-Cairo. Now she is studying the physical properties of graphene quantum dot and 2D materials for optoelectronic and room temperature gas sensors applications.

Mohamed A. Basyooni has completed his M.Sc. in Experimental Physical Chemistry with honors at Beni-Suef University in 2016. Now, he is a Ph.D. research student. He was working in semiconductor technology for many years to develop a room temperature gas sensor based on metal oxide semiconductors nanostructure thin films. Currently, he is working in ZnO, SnO_2, VO_2, MoS_2, WS_2 and graphene oxide for gas and biochemical sensors.

Mohamed Shaban is an associate professor and director of Nanophotonics and Applications Lab at Physics Department, Faculty of Science, Beni-Suef University. He received his Ph. D from Beni-Suef University through a scientific channel with Chonnam National University, South Korea from 2008 to 2010. His research interests include electrochemical, gas, optical, plasmonic, and SERS sensors; functional nanomaterials including thin films, nanoporous membranes, plasmonic nanostructures, nanoarrays and photonic crystals. He published 130 papers and contributes to 42 scientific research projects.

Mohamed Rabia received his M.Sc. degree from Beni-Suef University in 2015. He is currently an Assistant Lecturer at the Department of Chemistry, Faculty of Science, Beni-Suef University. His research interests are electrochemical sensor, gas sensors, functional polymer materials, solar cell, and hydrogen generation.

Yasin Ramazan Eker received his B.Sc., M.Sc. and Ph.D. from University D'Orleans-France. Dr Yasin Eker is assistant professor in Department of Metallurgical and Materials Engineering. During its PhD, he worked on the lithium-ion batteries anode materials (disordered carbons, carbon/silicone composites), moreover he synthesized carbon nanotubes by CVD methods. His postdoctoral fellows were focused on the development of activated carbon for symmetric supercapacitors in organic and in aqueous media. Presently, he is still working on electrochemical fields (dye sensitized solar cell, gas sensors) and carbon materials (activated carbon for pollutant adsorption, graphene synthesis by Hummers methods), but also on 2D materials, waste recovering and mechanical application of polymer-based composites.

Gamal Attia is full professor of physics and space sciences at space research lab in the National Research Institute of Astronomy and Geophysics-Cairo. He received his PhD from Moscow State University in applied physics. Currently, he is studying the space radiation effect on the nanoparticles for space solar cells and Mars gas Nano sensors.

Mucahit Yilmaz is currently an Assistant Professor in the field of experimental solid-state physics at Konya NEU University. Dr. Yılmaz has completed his Ph.D. in high temperature superconductors, then joint the Middle East Technical University in GÜNAM as a Postdoctoral Research Associate. Currently, he is focusing on functionalization of large-scale graphene, graphene oxide, Transition-metal Dichalcogenides and their gas sensing applications.

Ashour M. Ahmed got his Ph.D. degree from Beni-Suef University in physics. His current research interests are the fabrication of photonic crystal, plasmonic nanostructure and nanoporous material for different applications such as sensor, smart window, photocatalytic degradation, and hydrogen generation